SEARCH FOR STANDARD AND EXOTIC SUPERSYMMETRY SIGNATURES AT CMS*

Piotr Zalewski

on behalf of the CMS Collaboration

The A. Sołtan Institute for Nuclear Studies, Hoża 69, Warsaw, Poland

(Received June 1, 2010)

Representative subset of recent searches for low energy supersymmetry using CMS detector at LHC is presented. Novel techniques and background estimates directly from data are underlined to show CMS readiness to search for new physics using first LHC data.

PACS numbers: 14.80.Ly

1. Introduction

Supersymmetry is widely regarded as one of the most promising extensions of the Standard Model. During decades since its postulation we have learned a lot about supersymmetry except for one crucial aspect. We do not know if this symmetry is realized in the world of elementary particles [1]. One of the main goals of the experiments at Large Hadron Collider is to discover low energy supersymmetry if it exists in Nature. At the same time we hope to reveal the nature of the Dark Matter particle for which supersymmetry provides some very interesting candidates.

Physic performance of the CMS detector including sensitivity to supersymmetry was described in detail in Ref. [2].

The post Physics TDR results are published as CMS Physics Analysis Summary notes. In this paper a few representative examples of such studies are presented. Three are main stream analyses: multi-jet, di-photon and di-lepton searches and two are more exotic, in the sense, that they extend our search for new physics beyond original detector design to look at Heavy Stable Charged Particles flying through the detector or stopping in it.

* Presented at the Cracow Epiphany Conference on Physics in Underground Laboratories and Its Connection with LHC, Cracow, Poland, January 5–8, 2010.

2. Search strategy for exclusive multi-jet events

Missing energy is one of the most characteristic signatures of supersymmetry. However, it is also regarded as one suffering from huge QCD background due to mismeasurement of jet energy. The main goal of the analysis described in Ref. [3] is to extend the robust di-jet technique, first described in Ref. [4] and applied to CMS in Ref. [5], to include multi-jet event topologies. The idea is based on a use of a kinematic variable discriminating events with true missing energy from mismeasured ones without relying on purely calorimetric measurements which are susceptible to noise and to non beam backgrounds.

This robust analysis technique, very well suited to the early data, is based on the α_{T} variable, which is easy to define for a di-jet system.

$$\alpha_{\mathrm{T}} = \frac{E_{\mathrm{T}}^{j2}}{M_{\mathrm{T}}},$$

where

$$M_{\mathrm{T}} = \sqrt{H_{\mathrm{T}}^2 - \left(H_{\mathrm{T}}^{\mathrm{miss}}\right)^2}$$

and H_{T} is a scalar, whereas $H_{\mathrm{T}}^{\mathrm{miss}}$ is a vector sum of transverse jet energies.

Multi-jet systems are reduced to two pseudo-jets, by combining jets in a way to minimize the difference between scalar sums of transverse energy of jets forming each pseudo-jet.

For ideally measured event without missing energy $\alpha_{\mathrm{T}} = 0.5$. It could be seen in Fig. 1, that QCD background indeed peaks at that value for both di-jet and multi-jet topologies, whereas signal extends to the left, which allows to eliminate the QCD background very efficiently.

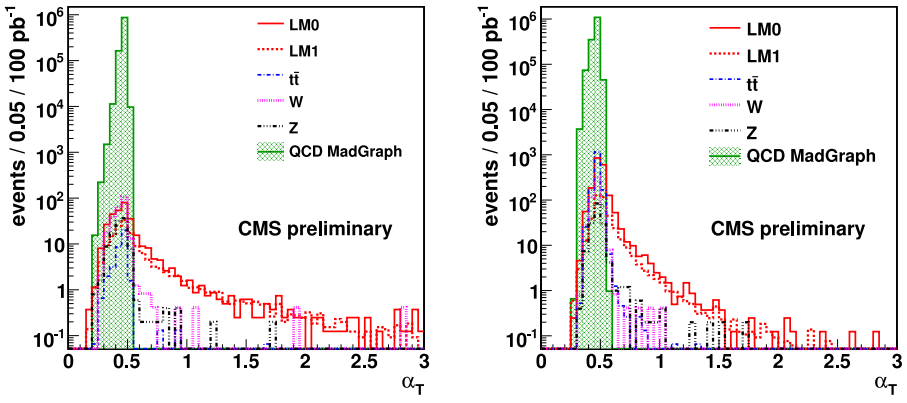

Fig. 1. Distribution of α_{T} for di-jet (left) and multi-jet (right) events. The number of events correspond to 100/pb at 10 TeV. Selection and data sets used are described in Ref. [3].

To establish the discovery of a SUSY signal it is necessary to be able to verify its incompatibility with SM background. For this purpose the $|\eta|$ of the leading jet could be used, because the signal events are expected to be produced more centrally than SM background, in particular the QCD one. In Fig. 2 one can see that the ratio of the number of events with α_{T} value above and below 0.55 is flat for background (right plot), whereas it grows with decreasing $|\eta|$ in a presence of the signal (left plot).

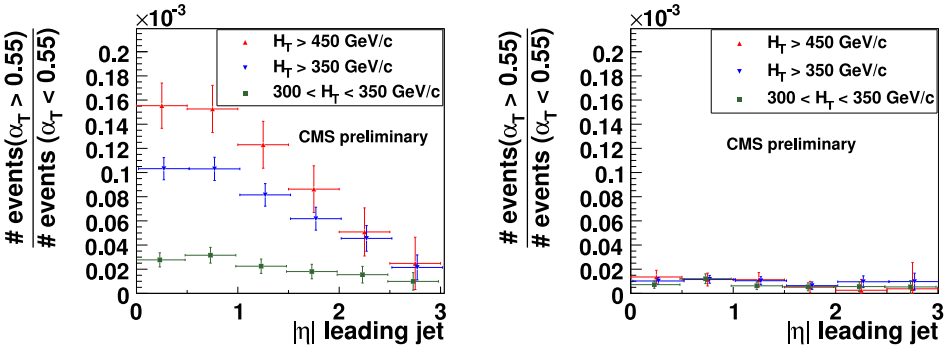

Fig. 2. Dependence of the ratio of the number of events with $\alpha_{\mathrm{T}} > 0.55$ to the number of events with $\alpha_{\mathrm{T}} < 0.55$ on $|\eta|$ of the leading jet for SUSY(LM0)+SM (left) and SM only (right) for 100/pb at 10 TeV.

Individual contributions to the background could be controlled in the following way.

- The QCD background after selection is expected to be negligible, but it could be further controlled using the last $|\eta|$ bin of the distribution shown in Fig. 2.

- The largest irreducible background, which is due to $Z+$jets events (with Z decaying to neutrinos), could be estimated using gamma+jets and $W+$jets events [6].

- In addition, highly boosted Ws from $W+$jets and $t\bar{t}$ events survive selection, when W decays to tau and its neutrino. This contribution could be evaluated by selecting $W \to \mu\nu$ decays and replacing reconstructed muons by simulated hadronic tau decays [7].

The idea to use kinematic variable α_{T} instead of $E_{\mathrm{T}}^{\mathrm{miss}}$ is very robust, especially for a search with early physics data. Several data control distributions have been identified [3]. These distributions (not discussed here) will allow an independent verification of the presence of a potential signal.

3. Data-driven background estimates for SUSY di-photon searches

A pair of high transverse energy photons with large missing energy $E_{\mathrm{T}}^{\mathrm{miss}}$ could signal new physics *e.g.* from gauge mediated supersymmetry breaking models (GMSB). Genuine background is small but there are three sources of instrumental background [8]:

- QCD: due to jet misidentification and $E_{\mathrm{T}}^{\mathrm{miss}}$ mismeasurements,
- EW: due to electron misidentification in events with genuine $E_{\mathrm{T}}^{\mathrm{miss}}$,
- and non-beam background.

Non-beam background is mainly due to electromagnetic cascades induced by cosmic and beam halo muons. To control these backgrounds the η width of the ECAL cluster and its timing could be used. It could be seen in Fig. 3 that the cluster timing of genuine gammas has low dispersion, value around zero and does not depend on η, whereas beam hallo induced signals show strong η dependence (two visible branches correspond to beam hallo muons originating from opposite proton beams) and much larger dispersion. Signals due to cosmic shows no correlation with pp timing. The η width of beam hallo induced EM clusters also depends on η (because of crystals pointing

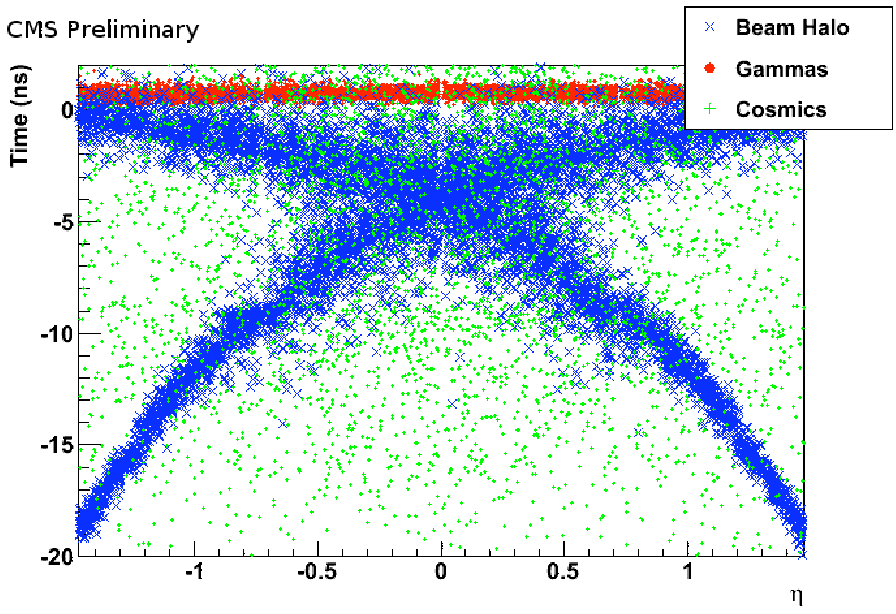

Fig. 3. Measured cluster time *versus* η for beam halo, cosmic and photon gun events. The samples are normalized to the same number of entries.

geometry) and is larger than for genuine photons, whereas the width of EM clusters due to cosmics is more dispersed. These differences not only allow for effective non-beam background reduction but also for precise estimate of the yields with data.

Selected ECAL clusters ($E_{\mathrm{T}} > 30\,\mathrm{GeV}$, isolation, η cluster width lower than 0.013, for details see Ref. [8]) are classified as electrons if they have pixel seed and photons otherwise.

The efficiency of pixel match is estimated using the ee sample to describe $Z \to ee$ peak and the $e\gamma$ sample to measure Z signal with one misidentified electron. The result is: $1 - f_{e\to\gamma} = (97,5 \pm 1.5)\%$, where $f_{e\to\gamma}$ is electron misidentification probability (not pixel matched electron is, by definition, regarded as photon). This probability will be reevaluated with real data. It is used to estimate EW and QCD backgrounds.

The contribution of the EW background to the $\gamma\gamma$ $E_{\mathrm{T}}^{\mathrm{miss}}$ distribution is determined using $e\gamma$ sample $E_{\mathrm{T}}^{\mathrm{miss}}$ distribution scaled by $f_{e\to\gamma}/(1 - f_{e\to\gamma})$.

Then QCD background $E_{\mathrm{T}}^{\mathrm{miss}}$ distribution is modeled using reweighted $Z \to ee$ sample selected with invariant mass cut ($80 < M_{ee} < 100\,\mathrm{GeV}$). Weights depend on transverse momentum p_{T} of di-EM system and are taken from the ratio of ee and $e\gamma$ distributions (Fig. 4). Weighted $E_{\mathrm{T}}^{\mathrm{miss}}$ distribution is normalized to $\gamma\gamma$ distribution for low $E_{\mathrm{T}}^{\mathrm{miss}} < 20\,\mathrm{GeV}$. The key assumption is that one could separate event into di-EM system, which is measured well, and recoil and other hadronic activity. This assumption cannot be derived from first principles but it was proved to hold using MC, and it could be verified using real multi-jet events with two jets dominated by neutral pions.

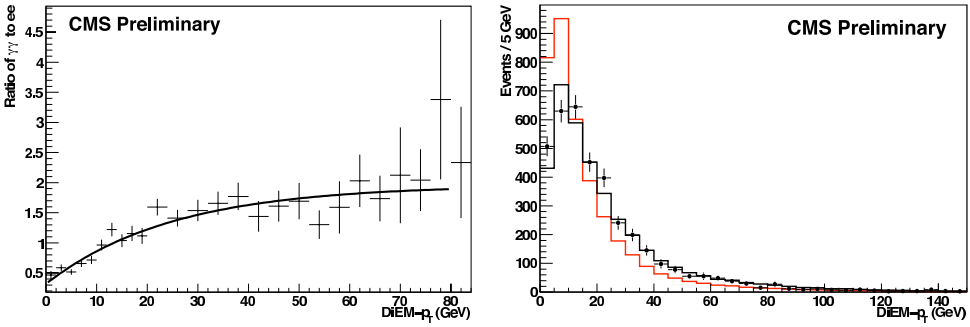

Fig. 4. Left: Ratio of di-EM p_{T} in $\gamma\gamma$ and $Z \to ee$) samples. Right: di-EM p_{T} distributions for $\gamma\gamma$ (points) and $Z \to ee$ (histograms) before and after reweighting.

In Fig. 5 the results of background closure test without signal and with GM1c signal mixed in are presented. One can observe very good agreement between data driven background estimate and background itself.

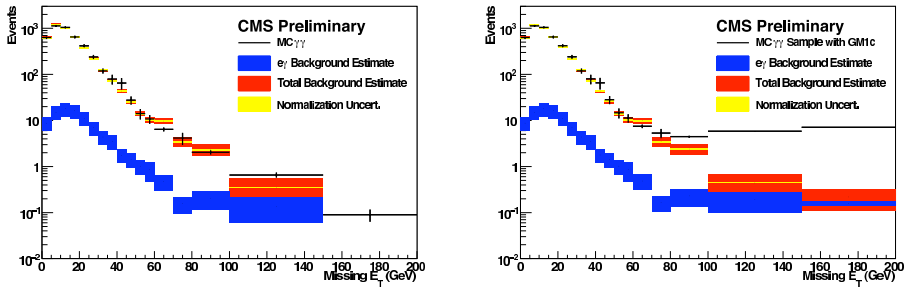

Fig. 5. Background closure test using $Z \to ee$ events to describe the QCD background. Left: without SUSY signal. Right: with GM1c SUSY. The last bin contains overflows. The number of events correspond to 100/pb at 10 TeV.

4. Di-lepton edge in SUSY

A leptonic decay of the next-to-lightest neutralino gives well known characteristic di-lepton edge signature of supersymmetry, which could allow to perform first mass difference measurements. The goal of the analysis [9] is to observe a significant excess of opposite sign same flavour (OSSF) lepton pairs over various backgrounds and to measure endpoint in the invariant mass distribution. All flavour symmetric background (including SUSY decays of this type) can be determined from data using opposite sign opposite flavour (OSOF) lepton pairs. However, even within mSUGRA model this decay can proceed in different ways. If there is a slepton with a mass in between two lightest neutralinos masses then two-body decay mode of second neutralino dominates and the endpoint can be expressed by

$$m_{\ell\ell}^{\max} = \sqrt{\frac{\left(m_{\tilde{\chi}_2^0} - m_{\tilde{\ell}}^2\right)\left(m_{\tilde{\ell}}^2 - m_{\tilde{\chi}_1^0}\right)}{m_{\tilde{\ell}}^2}}\,.$$

If not, then endpoint corresponds directly to neutralino mass difference (three-body decay). Finally, if neutralino mass difference matches Z or Higgs boson mass the shape of di-lepton edge could be distorted or invisible.

Because reconstruction efficiencies for muons and electrons differ, it is necessary to measure them from data. For this purpose "tag and probe" method is applied to leptonic Z boson candidates, where one lepton is used as a tag, whereas the efficiencies are measured for the second [10]. Invariant mass resolution is measured using leptonic Z decays as well, and parametrized, separately for muons and electrons, as a Gaussian with different widths on each side of the mode.

Events are selected requiring opposite sign pair of isolated leptons with transverse momentum of at least one of them above 16 GeV. On top of this a general SUSY signature of at least three jets with transverse momenta exceeding 100, 50 and 50 GeV and missing energy above 100 GeV is required.

Determination of the leptonic edge and number of signal events is done via unbinned extended maximum likelihood fit to di-lepton invariant mass distribution for both electrons and muons. As it was already stated all background which leads to uncorrelated lepton pairs can be measured directly from data [11]. Therefore, OSOF pairs of leptons are fitted simultaneously with OSSF pairs to recover common background probability density function having two-shape parameters. Signal parametrization appropriate for three-body or two-body decay is used depending on the goodness of the fit [9] and Z peak is fitted separately.

The result at LM0 benchmark point and integrated luminosity 200/pb at 10 TeV is shown in Fig. 6. The edge estimate reads: for three-body decay hypothesis: (52.8 ± 1.1)GeV (chi2/ndf=0.74); for two-body: (50.0 ± 1.8)GeV (chi2/ndf=0.79). Theoretical endpoint amounts to 52.7 GeV.

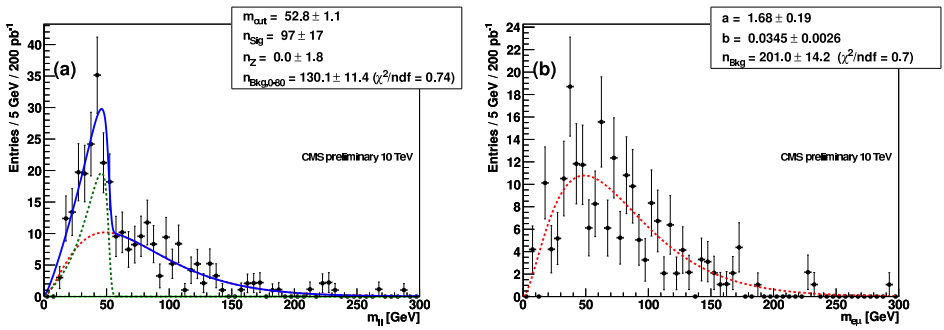

Fig. 6. The combined fit (common background shape) of OSOF (a) and OSSF (b) lepton pairs. The black points represent pseudo data corresponding to 200/pb of integrated luminosity at 10 TeV for LM0 benchmark point.

In Fig. 7 OSSF plots corresponding to the fits at LM9 (three-body decay) and LM1 (two-body decay) benchmark points for 1/fb at 10 TeV are shown. Integrated luminosity needed for 5σ signal significance (including systematics) with (and without) using shape of the di-lepton distribution information is estimated to 200/pb (250/pb) at LM0, 250/pb (400/pb) at LM1 and 350/pb (600/pb) at LM9.

The main challenge, however, will be the interpretation of di-lepton endpoint since it is difficult to distinguish statistically between two- and three-body decay with limited amount of data.

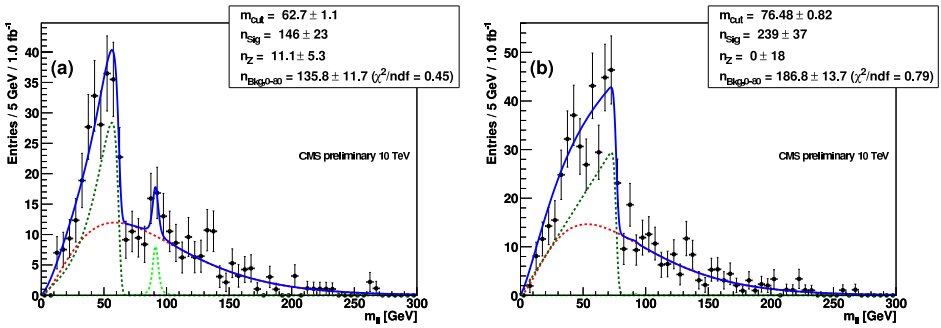

Fig. 7. The combined fit of OSOF (shown) and OSOF (not shown) lepton pairs at LM9 (a) and at LM1 (b) benchmark points. The black points represent pseudo data corresponding to 1/fb of integrated luminosity at 10 TeV.

5. Search for heavy stable charged particles

Existence of heavy stable charged particles (HSCP) is in contradiction with cosmological constraints, but models with such meta-stable particle are very intriguing and could be in agreement with all known constraints. A classic signature of HSCP is low-beta charged track. From the detector point of view HSCP is a muon-like track which could be late with respect to genuine muon of the same momentum and which could be highly ionizing. Class of HSCPs carrying color charge hadronize into so-called R-hadrons and could change electric charge during passage through a detector giving even more strange signatures. For review on HSCP phenomenology see *e.g.* [13].

The strategy is to search for highly penetrating tracks which are late (with respect to muons) and highly ionizing. LHC detectors were not designed to perform such tasks, but fortunately enough, there is a lot of possibilities to be used. Historically, the first attempt to extract HSCP signal at LHC was done more than a decade ago [14] using barrel muon system of the CMS detector which is equipped with layers of drift tubes (DT) measuring muon position via drift time measurement. An off-time particle gives wavy pattern in staggered DT layers instead of straight line, allowing for arrival time measurement with a precision of about 2 ns per single superlayer consisting of four DT layers. Other subdetectors that allow for a time measurement in the CMS detector are: both calorimeters and cathode strips chambers (CSC) present in the forward muon system. In all these detectors time measurement is possible because the pulse is probed several times to allow for precise determination of energy or position. The precision of time measurement ranges from about half a ns for ECAL to a few ns for CSC. Some limited time sensitivity is provided by resistive plate chambers (RPC)

which completes muon trigger system. There is ongoing feasibility study on redesigning RPC trigger firmware to allow for triggering on very low velocity HSCP.

As far as the ionization measurement in the CMS is concerned, it is possible in the tracker and in both calorimeters.

Publicly available analysis [12] is based only on the Time of Flight (TOF) measurement with drift tubes (DT) system and specific ionization measurement with silicon tracker. Both measurements are used to determine inverse beta $\beta^{-1} = (v/c)^{-1}$ which, when combined with momentum measurement, allows for particle mass determination. The idea of β^{-1} from TOF measurement is the following

$$\beta_{\mathrm{DT}}^{-1} = \frac{c\,\delta t}{L} + 1\,,$$

where L is the flight distance and δt is the time delay with respect to relativistic muon.

In the silicon tracker, typical track is associated with about 15 energy measurements giving good estimate of the most probable value (MPV) dE/dx. For low beta particles dE/dx is proportional to β^{-2} and one can measure

$$\beta_{\mathrm{Tk}}^{-1} = \sqrt{K\frac{dE}{dx}}\,,$$

where constant K can be obtained directly from data using low momentum protons and kaons.

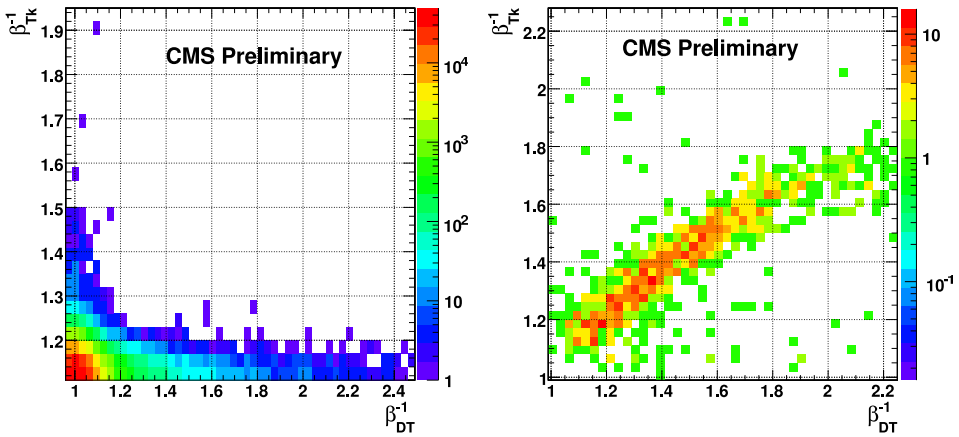

Fig. 8. Inverse beta estimate via dE/dx in the tracker *versus* estimate via TOF in the DT muon system for 1/fb. Left: background. Right: signal: stop 500 GeV.

In Fig. 8 the synergy of two independent β^{-1} estimates is demonstrated. Simple cuts on both estimates after applying some quality requirements [12] to muon candidates above $p_{\mathrm{T}} > 30\,\mathrm{GeV}$ reduce background by an adjustable factor of the order of 10^7. The working point will be chosen after inspection of real data tails for lower transverse momenta muons.

In Fig. 9 integrated luminosity needed to select 3 events, for different types of signal models (see the legend) as a function of HSCP mass for $\sqrt{s} = 14\,\mathrm{TeV}$ is shown in the left plot, whereas in the right plot the same lines are rescaled to $\sqrt{s} = 7\,\mathrm{TeV}$ using parton luminosity ratio. For integrated luminosity of 200/pb at 7 TeV an evidence for GMSB stau with mass around 200 GeV, stop with mass around 500 GeV and gluino with mass around 800 GeV could be found if any of these particles exist in nature.

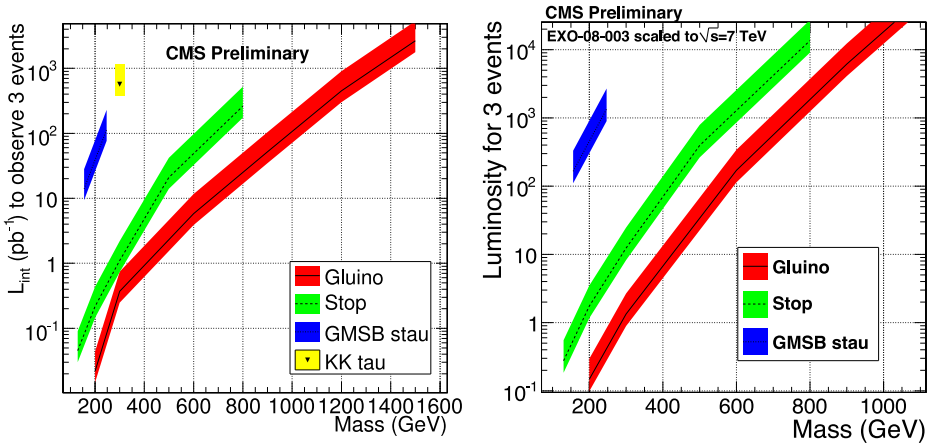

Fig. 9. Integrated luminosity needed to select 3 events, for different types of signal models (see the legend) as a function of HSCP mass for $\sqrt{s} = 14\,\mathrm{TeV}$ (left) and rescaled to $\sqrt{s} = 7\,\mathrm{TeV}$ using parton luminosity ratio (right).

6. Search for stopped gluinos during beam-off periods

The least energetic HSCPs will stop in the detector, and decay asynchronously. In the analysis [15] a search strategy for such decays is described. Although the search is generic, the Split SUSY [16] is used as a benchmark signal. In this model, the gluino is long lived, because it may decay only via a highly virtual squark and it will hadronize as R-hadron. As in other SUSY models, the gluino production cross-section at LHC is expected to be large.

In Fig. 10 the distributions of gluino stopping points inside CMS are shown. Since these subsequent decays of stopped gluinos are out-of-time with respect to LHC collisions it is possible to search for them during periods in the LHC orbit when there are no collisions (beam-gaps) or periods when there is no beam in the machine (inter-fill periods), to avoid beam induced background.

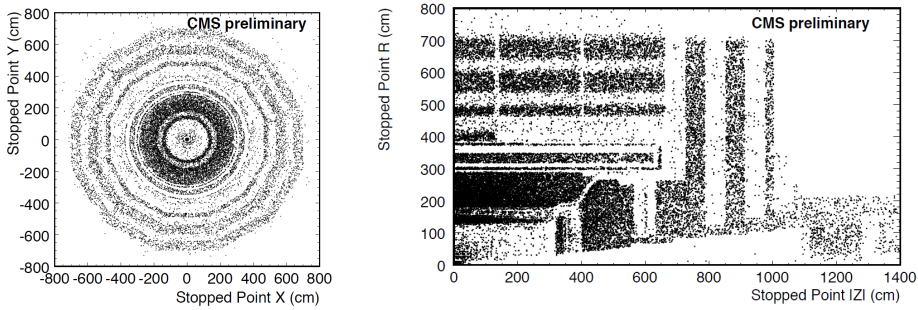

Fig. 10. R-hadron stopping points for $m_{\tilde{g}} = 300\,\text{GeV}$ and $\sqrt{s} = 10\,\text{TeV}$.

Most of R-hadrons stopping in the CMS will stop in the calorimeters, mainly HCAL. In the left plot in Fig. 11 shadowed histogram shows R coordinate at stopping point, whereas hollow dashed histograms correspond to gluinos decays giving more than 5 GeV deposit in the ECAL or in both calorimeters. Such deposit could be used for trigger during beam-off periods. The right plot in the same figure shows gluino stopping efficiency for conservative (electromagnetic interaction only) and optimistic (nuclear interaction dominate) assumption about R-hadron interaction with matter.

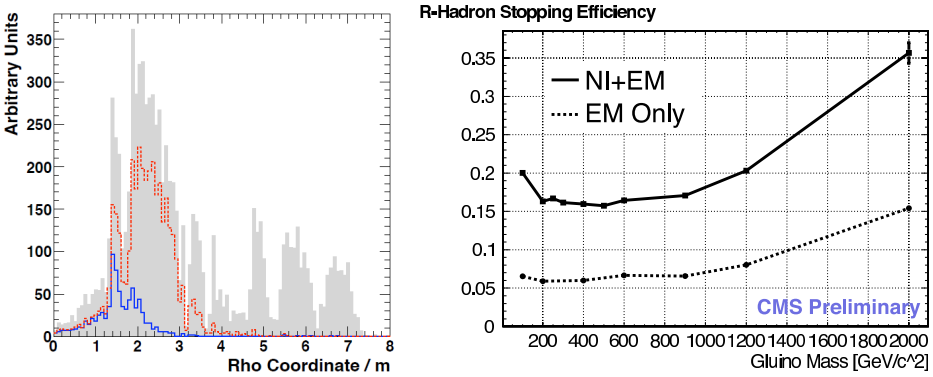

Fig. 11. Left: Rho coordinate of R-hadron stopping points for $m_{\tilde{g}} = 300\,\text{GeV}$ and $\sqrt{s} = 10\,\text{TeV}$. Right: probability of stopping R-hadron anywhere in the CMS in function of the gluino mass.

L1 trigger is defined as the logical AND of *(i)* the lowest threshold (10 GeV) normal jet trigger with *(ii)* the no beam condition bit. During cosmic runs the L1 rate was measured to be 200 Hz. To reduce this rate further, at the HLT level, noisy HCAL channels are filtered out, jets are reconstructed and 20 GeV threshold applied to the leading jet energy. Cosmic veto is applied off line. The rate was measured to be less than 10 Hz, and relative efficiency is expected to be around 30%.

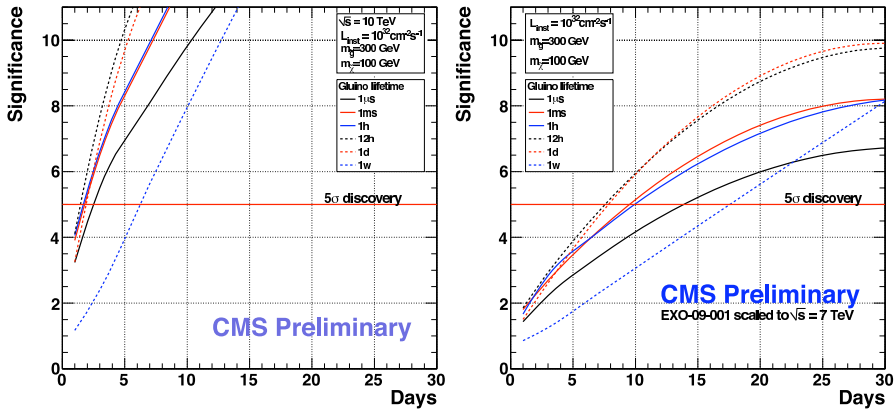

Fig. 12. Discover ability using both beam gaps and inter-fill periods in a combined counting experiment for gluino mass 300 GeV, neutralino mass 100 GeV and different gluino lifetimes. Left: for $\sqrt{s} = 10$ TeV. Right: rescaled to $\sqrt{s} = 7$ TeV using parton luminosity ratio. Assumes instantaneous luminosity of 10^{32} cm^{-2}. The 1 ms curve is representative for a range of lifetimes from 10 μs to 100 s.

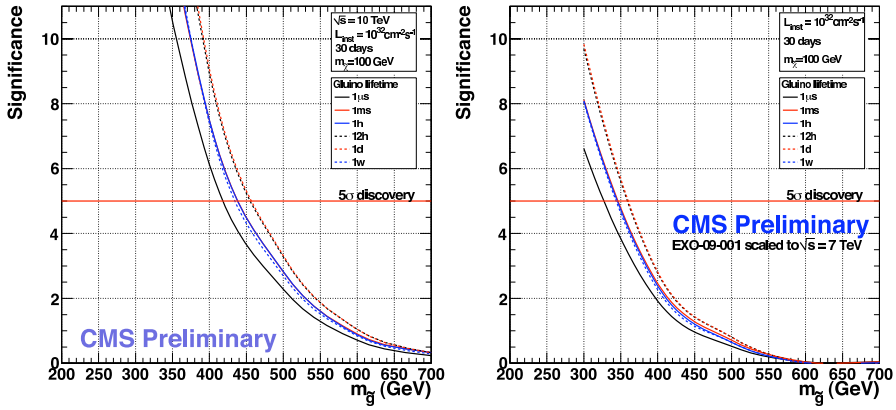

Fig. 13. Significance achievable after 30 days running at instantaneous luminosity of 10^{32} cm^{-2} as a function of gluino mass for neutralino mass 100 GeV and different gluino lifetimes. Left: for $\sqrt{s} = 10$ TeV. Right: rescaled to $\sqrt{s} = 7$ TeV using parton luminosity ratio.

Expected results are shown in Figs. 12 and 13 for different gluino lifetimes at instantaneous luminosity of $10^{32}\,\mathrm{cm}^{-2}$, using both beam gaps and interfill periods in a combined counting experiment for $\sqrt{s} = 10\,\mathrm{TeV}$ (left) and rescaled to $\sqrt{s} = 7\,\mathrm{TeV}$ using parton luminosity ratio (right). The 1 ms curve is representative for a range of lifetimes from $10\,\mu$s to 100 s.

7. Summary

A representative subset of recent searches for low energy supersymmetry using CMS detector at LHC was presented. All analyses are based on the use of the first data to control and measure background. Even with very limited amount of data to be recorded during the first period of LHC running at high energy CMS is able to discover supersymmetry if it exists and sparticle masses are just above current experimental limits. Presented analyses were performed mainly for $\sqrt{s} = 10\,\mathrm{TeV}$, but updates for $\sqrt{s} = 7\,\mathrm{TeV}$ are to be publicly delivered and some of them are already included in the present paper.

I would like to thank organizers of the Cracow Epiphany Conference for invitation and hospitality. This work was supported in part by the Polish Ministry of Science and Higher Education Grants N N202 230337 and 666/N-CERN/2010/0.

REFERENCES

[1] S.P. Martin, `hep-ph/9709356`.
[2] [CMS Collaboration], *J. Phys. G: Nucl. Part. Phys.* **34**, 995 (2006).
[3] [CMS Collaboration], CMS PAS SUS-09-001.
[4] L. Randall, D. Tucker-Smith, *Phys. Rev. Lett.* **101**, 221803 (2008).
[5] [CMS Collaboration], CMS PAS SUS-08-005.
[6] [CMS Collaboration], CMS PAS SUS-08-002.
[7] [CMS Collaboration], CMS PAS HIG-08-001.
[8] [CMS Collaboration], CMS PAS SUS-09-004.
[9] [CMS Collaboration], CMS PAS SUS-09-002.
[10] [CMS Collaboration], CMS PAS EGM-07-001.
[11] [CMS Collaboration], CMS PAS EGM-08-001.
[12] [CMS Collaboration], CMS PAS EXO-08-003.
[13] M. Fairbairn, A.C. Kraan, D.A. Milstead, T. Sjöstrand, P. Skands, T. Sloan, *Phys. Rep.* **438**, 1 (2007).
[14] M. Kazana, G. Wrochna, P. Zalewski, CMS CR-1999/019.
[15] [CMS Collaboration], MS PAS EXO-09-001.
[16] N. Arkani-Hamed, S. Dimopoulos, *J. High Energy Phys.* **06**, 073 (2005).